JOURNAL OF MATERIALS SCIENCE 13 (1978) 377–390

The stiffness and strength of a polyamide thermoplastic reinforced with glass and carbon fibres

P. T. CURTIS, M. G. BADER, J. E. BAILEY
Department of Metallurgy and Materials Technology, University of Surrey, Guildford, UK

It has been established that the optimum degree of mechanical property enhancement by fibre reinforcement of a typical thermoplastic material (polyamide 6.6) is achieved if comparatively long fibres are used, the fibre length required being determined by the properties of the interface between the fibre and the thermoplastic matrix. The extent of stiffness improvement at low strains is described by simple modifications to the law of mixtures to allow for fibre orientation and length. The strength enhancement is limited by an embrittlement effect which reduces the strain to fracture as the stiffness of the composite is improved. The cause of this effect has been identified as matrix crack formation at the ends of the reinforcing fibres. At strains of between 0.5% and 1.0%, according to fibre type, length and V_f, cracks form at the tips of the longest fibres aligned in the straining direction. Subsequently as the strain is increased more cracks form progressively at the ends of shorter and/or more misaligned fibres. It has been shown that initially this cracking can be accommodated by load transfer to adjacent fibres which "bridge" the cracked region. Final failure occurs when the extent of cracking across the weakest section reaches a critical level when the surrounding fibres and matrix can no longer support the increasing load.

1. Introduction

When thermoplastics are reinforced with short fibres, both stiffness and strength may be increased and the extent of this improvement is a function of the fraction of fibres, their length and their orientation. In general the greatest improvements in mechanical properties are obtained with high volume fractions of long fibres aligned in the test direction. However, both the V_f and length of fibre which may be incorporated into practical thermoplastic systems are limited by the requirements for adequate melt flow during the moulding or shaping operations. There is also an embrittling effect which reduces the strain to failure in the more highly reinforced materials and this effect limits the extent of strength improvement [1–3].

In the present work an experimental study of glass and carbon fibre-filled polyamide has been undertaken with the particular aim of improving our understanding of the failure process. A programme of mechanical testing backed up by detailed structural studies has indicated that failure in highly reinforced materials occurs by progressive matrix cracking and this concept has been used to develop a revised model for composite stiffness and strength applicable to discontinuous fibre systems.

1.1. List of symbols

A_s = Area of a single matrix crack,
C = fibre orientation constant,
E_c = composite modulus,
E_m = matrix modulus,
E_f = fibre modulus,
L = fibre length,
$\bar{L}$ = mean fibre length,

L_e = critical fibre length at a composite strain ϵ_c,
V_f = fibre volume fraction,
V_m = matrix volume fraction,
V_f^{eff} = effective fibre volume fraction,
V_m^{eff} = effective matrix volume fraction,
q_B = number of bridging fibres,
q_C = number of fibre ends,
r_f = fibre radius,
r_s = matrix crack radius,
ϵ_c = composite strain,
$_{1,2}\epsilon_c$ = composite strain at Stage 1 to 2 transition,
ϵ_f = fibre strain,
ϵ_i = crack initiation strain,
ϵ_m = matrix strain,
ϵ_{uc} = ultimate composite strain,
θ = fibre angle,
σ_f = fibre stress,
σ_{uf} = ultimate fibre stress,
σ_{uc} = ultimate composite stress,
σ_m = matrix stress,
τ = fibre/matrix bond shear strength.

2. Experimental procedure

2.1. Material compounding and injection-moulding

The principal raw materials used in this investigation are listed in Table I. An injection-moulding compound was prepared by extrusion-coating continuous fibre rovings with the polymer using a technique developed and described elsewhere [1–4]. The coated fibre tows were chopped into 6 mm pellets for subsequent injection-moulding. This technique had the advantage of retaining long fibres in the moulding pellets, and consequently in the finished material, whereas commercially available compounds contained only very short fibres. Moulding compounds with shorter fibres were made by re-extruding the original moulding pellets. The compounds were moulded into test pieces with V_f from 0 to 0.2 using screw-preplasticizing injection-moulding machines. The bulk of the work utilized a semi-automatic machine, but in the later stages of the project a fully automatic machine became available. Tensile and impact test pieces were moulded simultaneously in a multi-cavity mould, the tensile test-piece having a gauge portion 40 mm long and 5 mm x 2 mm in section. High V_f materials required higher moulding temperatures and pressures to obtain adequate melt flow to fill the mould cavities, but care was taken to minimize polymer degradation by using the lowest possible temperatures and reducing the residence time of the material in the hot end of the machine. Moulding was therefore carried out over a temperature range from 270 to 305° C depending on V_f. The commercial Maranyl A190 material was also moulded, a range of V_f being obtained by diluting the pellets with unfilled PA66 in the machine hopper.

In all, six series of moulding compounds were prepared, each with a range of V_f. The designations used for these compounds are given in Table II.

TABLE I List of raw materials.

Material	Commercial Description	Suppliers	Comments
Polyamide 6.6	Maranyl A100	ICI Plastics Ltd.	Matrix Polymer
Glass fibre/ PA.66	Maranyl A190	ICI Plastics Ltd.	A commercial glass filled polyamide $V_f = 0.18$
Glass fibre	FGRE 1	Fibreglass Ltd.	Treated with size MSS1421 compatible with PA.66 4600TEX
Carbon fibre	Modmor type II-S	Morganite Modmor Ltd.	Surface treated fibres prepared from PAN precursor 940TEX

TABLE II List of moulding compounds prepared

Designation	Description
1. LGN	"Long" glass fibres in polyamide 6.6 matrix, average fibre length, L = 0.5 mm, V_f up to 0.2.
2. SGN	Short glass fibres in PA6.6 LGN re-extruded to break down fibres $\bar{L} = 0.27$ mm V_f up to 0.2.
3. CGN	Commercial filled PA6.6 (Maranyl A190) based compound $\bar{L} = 0.2$ mm V_f up to 0.18.
4. LCN	Long carbon fibres in PA6.6 $\bar{L} = 0.4$ mm, V_f up to 0.2.
5. SCN	Short carbon fibres in PA6.6 LCN re-extruded to break down fibres, $\bar{L} = 0.25$ mm, V_f up to 0.2.
6. VSCN	Very short carbon fibres in PA6.6 LCN re-extruded at least twice, $\bar{L} = 0.2$ mm, V_f up to 0.2.

2.2. Mechanical testing

The injection-moulded testpieces were conditioned prior to testing by storing at 20° C and approximately 50% r.h. for a period of 21 days, this being particularly important for the hygroscopic polyamide since its properties are sensitive to water content. All tensile tests were performed on an Instron TTD machine with an Instron strain gauge extensometer, at a constant crosshead extension rate of 0.2 mm min^{-1} (strain rate $\approx 10^{-4}$ sec^{-1}). A direct force/strain plot was produced using the chart-servo-drive mechanism linked to the extensometer. The composite modulus E_c was taken at an arbitrary strain of 0.005, this being termed the 0.5% secant modulus. In addition to the stiffness, E_c, the maximum stress, σ_{uc}, and the failure strain ϵ_{uc} were recorded for each material tested.

2.3. Acoustic emission analysis

An acoustic emission monitoring system has been used to supply additional information on failure behaviour. This consisted of a high frequency piezo-electric sensor clamped to the gauge-portion of the test piece and a high-gain amplifier which recorded sounds emitted by specimens under test. The equipment was used during a normal tensile test, the number of acoustic events was recorded as a cumulative plot at the same time as was the force/extension data.

A wide range of the filled PA.66 samples were so tested. In all cases the total acoustic count and the specimen strain at one hundred counts was recorded and the relationship between the stress/strain curves and acoustic output was correlated. The extent of random noise pickup was checked by operating the equipment on the most sensitive range for long periods of time, very few counts being recorded. Tests on unfilled PA.66 over similar strain ranges to those used for the filled materials also showed very few counts. It was noted that the point of fracture was preceded by a marked increase in the count rate, so that tests could be stopped and specimens unloaded for examination just prior to the final fracture sequence of events.

2.4. Microscopy and length distribution analysis

Longitudinal and transverse sections of mouldings were prepared and examined using conventional reflection optical microscopy techniques and fracture surfaces examined by scanning electron microscopy.

Fibre length distributions were determined by releasing fibres from samples cut from mouldings by chemical digestion in a mixture of hot concentrated sulphuric acid and hydrogen peroxide [5]. Then, after washing, the fibre residue was filtered onto filter paper discs. After drying, the fibres were examined and photographed under an optical microscope. This enabled a general visual comparison of fibre lengths to be made.

As well as this simple comparative analysis, a more detailed analysis was undertaken on selected samples to obtain exact fibre length distributions. Photomicrographs of released fibres were prepared and the individual fibres were measured and counted; between 1000 and 2000 fibres were counted for each sample. These length distributions. were determined for both long and short carbon and glass fibre compounds of 0.1 V_f.

In order to ascertain whether an appreciable number of fibres broke during loading up to fracture, distributions for both untested and fractured samples were measured. This involved chemically releasing fibres from a portion of the tested specimen adjacent to the fracture point and from an unstrained sample taken from the end portion of the same test piece. In this way, errors due to variations in V_f or fibre distribution between samples were minimized.

3. Results

A typical stress/strain curve for a LCN specimen is shown in Fig. 1, together with the curve derivative. This shows a three-stage behaviour, and was observed in all the fibre-filled materials, although the slopes and durations of the stages varied. The first stage is linear and its extent was measured for each material from the curve derivatives, the transition to Stage 2 being well defined. Stage 2 is parabolic but Stage 3 cannot be described by a simple model, since the transition was gradual and not clearly defined. Table III gives the mean Stage $1 \rightarrow 2$ transition strains for the range of materials tested; values of this parameter were found to be higher for the glass than for the carbon fibre system and also higher for longer fibre materials, although little dependence on V_f was observed. The second derivatives of the stress/strain curves in the Stage 2 region were also measured (Table III). In general the extent of

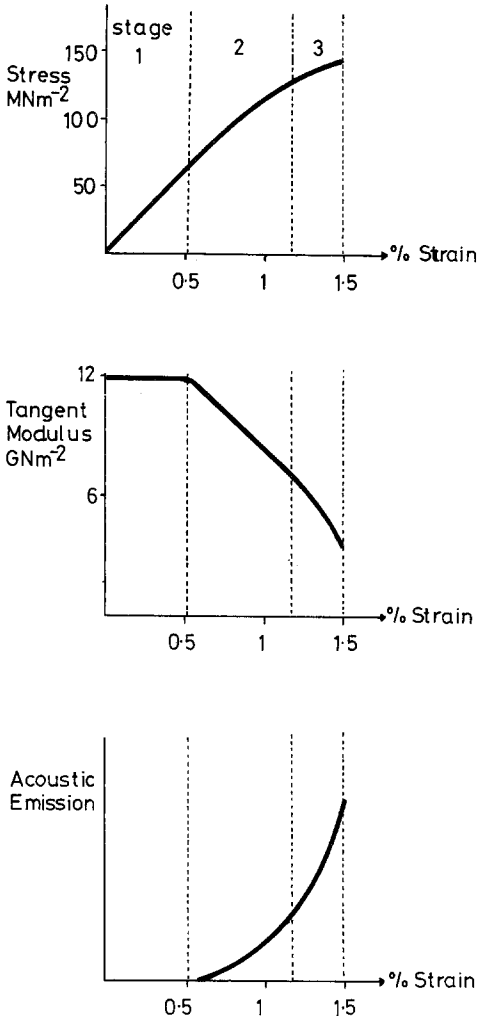

Figure 1 Typical tensile behaviour of a 10% carbon fibre/PA.66.

Stage 3 was least in the most brittle materials (the high V_f LCN material) and increased with decreasing V_f, fibre modulus and fibre length, as indicated in Table III. In very low V_f materials (less than 0.05) the three stages were very difficult to distinguish.

The unfilled polymer showed a linear stress/strain relationship over the strain range revelant to the filled materials and one may thus regard it as virtually Hookean in this context. The unfilled polymer when moulded at conventional temperatures (265 to 270° C) exhibited a well defined yield point at a strain of 5.8% showing extremely ductile behaviour and strained to over 100% before failure. In contrast when moulded at 300° C it failed in a brittle manner at a strain of

TABLE III Three stage parameters of FRTP stress/strain curves

Material	Strain at stage 1→2 transition (%)	Stage 2 rate of slope change ($GN\,m^{-2}$)	Extent of stage 3
LCN $V_f = 0.2$	0.52 ± .06	−860 ± 70	Very short
LCN $V_f = 0.1$	0.50 ± .06	−590 ± 50	Short
SCN $V_f = 0.1$	0.33 ± .06	−565 ± 50	Moderate
VSCN $V_f = 0.1$	0.30 ± .05	−500 ± 50	Long
LGN $V_f = 0.17$	0.80 ± .05	−280 ± 30	Long
SGN $V_f = 0.2$	0.45 ± .03	−260 ± 30	Long
SGN $V_f = 0.1$	0.50 ± .06	−170 ± 20	Long
CGN $V_f = 0.18$	0.39 ± .03	−240 ± 40	Very long

4.9% and a stress of 71 $MN\,m^{-2}$, which can be compared with the yield stress of the conventional polymer (69 $MN\,m^{-2}$). This is important since it implies that the matrix may well be quite brittle due to the high temperatures required to mould the filled materials. The relationship between 0.5% secant modulus and V_f (Fig. 2) was approximately linear, although at high V_f increased fibre alignment (discussed later) resulted in relatively higher moduli in the high-V_f long-fibre materials. The characteristic slope observed in Fig. 2 for each of the filled materials tested can be accounted for in terms of the inherent stiffness of the fibre and the mean fibre length. All the highly filled materials tested failed in a brittle manner. Carbon fibre-filled specimens had lower failure strains than those filled with glass (Fig. 3) and the longer the mean fibre length and the higher the V_f, the lower was the failure strain. All ma-

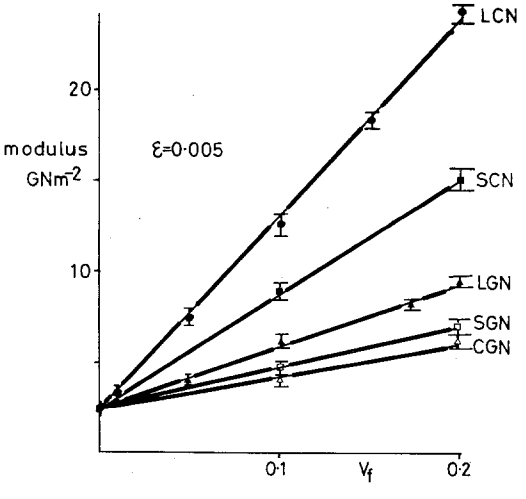

Figure 2 Secant modulus versus V_f.

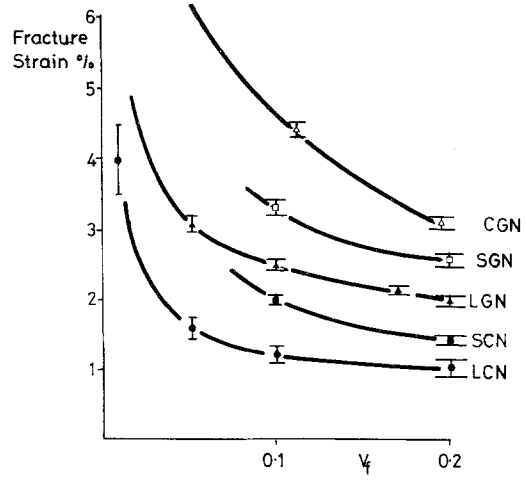

Figure 3 Fracture strain versus V_f.

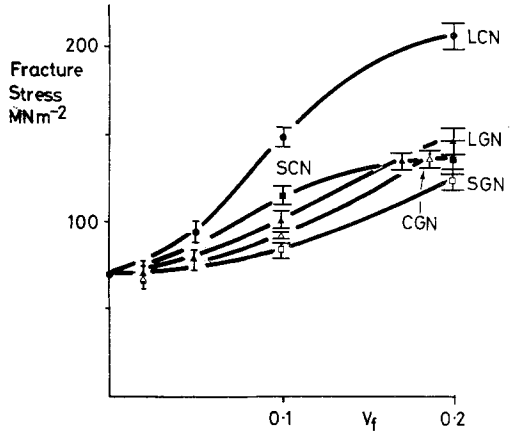

Figure 4 Fracture stress versus V_f.

terials, apart from those with very low fibre contents, failed at strains below the yield strain of the unfilled matrix (5.8%), and in the high-V_f long-fibre materials at strains lower than the fibre failure strains (~ 1.3% for type 2 carbon fibres and 3% for *E*-glass fibres). In very low V_f specimens (V_f less than 0.02 in the carbon- and 0.03 in the glass-filled materials) a different behaviour was observed and failure occurred in a ductile fashion at much higher strains, sometimes in excess of 10%. Polymer drawing was then observed on a microscopic but not on a macroscopic level. (Lower V_f specimens were moulded at lower temperatures, when the matrix might be expected to be more ductile). The ultimate strength (Fig. 4) was improved by fibre-filling apart from an initial drop at low V_f in some systems.

Fig. 5 shows the range of fibre lengths encountered in the filled materials tested. The recycling operation used to produce short fibre materials was indeed shown to further reduce fibre lengths, although the fibres were still longer than in the commercial material, this being reflected in the mechanical properties of the composites. The modulus of the SGN material is higher than that of the CGN., however, the CGN appears stronger due to its greater strain at fracture. It is apparent from Fig. 5a that substantial fibre break-up occurs during the injection-moulding operation as all the fibres were ~ 6 mm long in the granules fed into the machine. A typical full fibre length distribution for LCN is shown in Fig. 6 (similar data for all four materials is presented elsewhere [4, 6]. Mean fibre lengths were

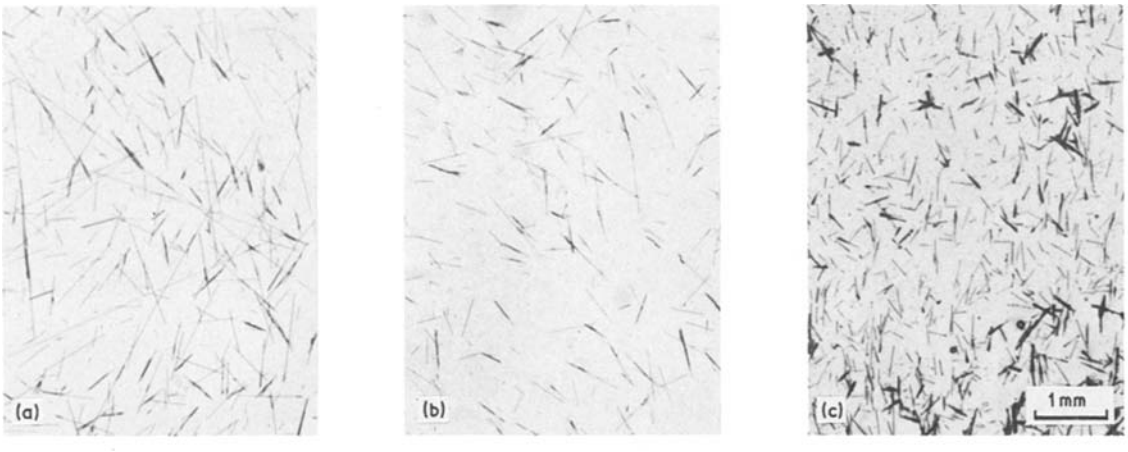

Figure 5 Comparison of fibre lengths in injection-moulded LCN, SCN, and CGN; (a) LCN, (b) SCN, (c) CGN.

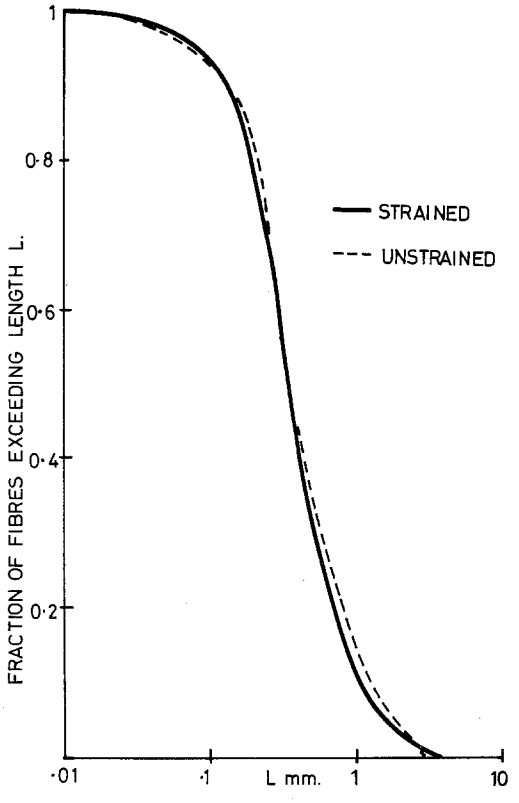

Figure 6 Cumulative length distribution for strained and unstrained LCN.

calculated on a volume basis (i.e. that length which half the volume of fibres exceeded) and shown to be 0.4 and 0.25 mm for the carbon materials and 0.5 and 0.27 mm for the glass materials. The "long" fibre samples however had a much greater proportion of very long fibres (i.e. those exceeding 2 mm). Random scatter of the mean, determined from samples from the same moulding run, was 5 to 10%, although larger variations were detected between specimens from different runs due to variations in moulding conditions which affected the degree of fibre attrition. No significant change was observed in the fibre length distributions before and after fracture, as shown in Fig. 6 for LCN in which strained and unstrained portions of a broken test-piece are compared. It was possible that some of the very long fibres had been broken, since the number of these in any one sample would be small and this portion of the distribution would be very sensitive to sample differences. The variation of 5 to 10% observed in the distribution mean-length also limits the minimum detection threshold for this technique; so that more than about 20% of the longer fibres must have been broken before a positive result could have been obtained. It may be concluded, however, that no gross fibre fracture occurred during loading to the fracture strain.

TABLE IV Acoustic emission data.

Material	Strain at 100 Counts (%)	Range of Maximum Counts $\times 10^3$
LCN $V_f = 0.2$	0.48 ± 0.04	15 → 50
LCN $V_f = 0.1$	0.57 ± 0.05	20 → 75
SCN $V_f = 0.1$	0.64 ± 0.06	60 → 90
VSCN $V_f = 0.1$	0.69 ± 0.09	30 → 100
LGN $V_f = 0.17$	0.90 ± 0.05	20 → 30
CGN $V_f = 0.18$	0.88 ± 0.05	20 → 120
CGN $V_f = 0.11$	1.02 ± 0.08	160 → 180
CGN $V_f = 0.055$	1.75 ± 0.10	140 → 200

Although the fibre length distribution measurements lead to the conclusion that substantial fibre fracture does not occur, pronounced acoustic emission is recorded, as shown in Fig. 1. Curves of similar form were obtained for all materials tested, acoustic output commencing in the Stage 2 region and accelerating rapidly with increasing specimen strain. Values of the total accumulated count varied substantially with failure strain and also with the distance between the transducer and the fracture point, due to attenuation within the material. Thus the actual numbers are of little significance. Typical results are given in Table IV in which the range of total counts and the strain for 100 recorded counts are presented (this was taken as an arbitrary criterion for the onset of specimen damage). Since gross fibre fracture does not occur, the substantial acoustic emission indicates that an alternative noise generating source, such as matrix cracking or fibre debonding, is operative.

Optical reflection microscopy showed pronounced alignment of fibres along the flow direction in all cases (Fig. 7) being most marked in high V_f long-fibre and least in low V_f short-fibre specimens, the fibres close to the specimen surface were found to be less well aligned. No obvious change with depth was observed apart from this surface effect. Very few fibre fractures were

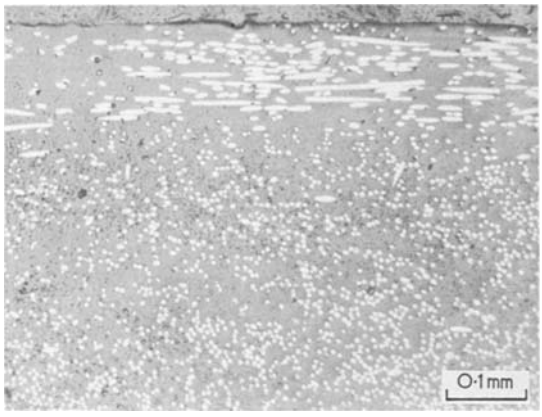

Figure 7 LCN section perpendicular to the specimen axis.

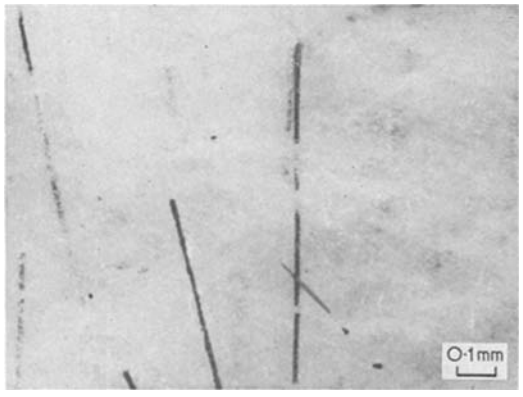

Figure 8 Subsurface fibre fracture in low V_f LCN.

detected in either glass or carbon filled materials which had failed at low strain (i.e. the higher V_f materials) despite a very exhaustive study of both surfaces and sections of broken test pieces. However, in low V_f specimens that failed in a more ductile fashion, abundant fibre fracture was observed, as shown in Fig. 8. The fracture mechanism thus changes from a brittle mode involving little fibre fracture at high V_f to a ductile one with considerable fibre fracture at low V_f.

All specimens failing in the brittle fashion showed abundant matrix cracking, particularly in the region close to the main fracture. Fig. 9 shows a typical area in a fractured LCN specimen showing many matrix cracks but no fibre fractures. In contrast, no matrix cracking was observed in the ductile low V_f specimens. No damage was observed in Stage 1 but in the second half of the Stage 2 region, after the onset of the acoustic count, minute matrix cracks were observed in the

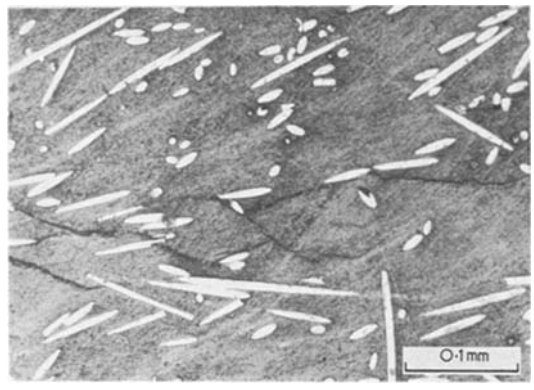

Figure 9 Matrix cracking in LCN.

material. In Stage 3 matrix cracks were far more abundant and there appeared to be a correlation between matrix cracking and acoustic output; the higher the recorded noise count, the more abundant the matrix cracking. In specimens examined prior to failure, matrix cracks were observed more than a few fibre radii in length, although after fracture much longer cracks were found.

The CGN specimens behaved in a slightly different manner, matrix cracking being much less prominent, although very little fibre fracture was observed. Acoustic output was very high in these specimens, implying that the source of noise might not be matrix cracking but perhaps fibre debonding. Unfortunately, it has not been possible to confirm this hypothesis.

Unfilled PA.66 moulded at the higher temperatures was observed to fail at low strains and this was reflected in the brittle nature of the fracture surfaces (Fig. 10a). Fibre-filled materials failing also showed this very brittle matrix behaviour (Fig. 10b). Extensive fibre pull-out was observed and the pull-out lengths were longer in the glass filled materials. Considerable matrix debris was observed on fibres and fibre ends, particularly in carbon-filled systems, indicating good fibre/matrix adhesion (Fig. 11). In low V_f (0.02) LCN specimens which failed in a brittle fashion radial markings were observed, the source of which appeared to be fibre ends (Fig. 10b). This suggests that the fibre ends are possible crack initiators. Low V_f specimens that failed in the ductile fashion displayed entirely different behaviour, considerable microdrawing being observed (Fig. 12). The CGN material whilst generally similar to the other highly filled materials, showed some matrix flow.

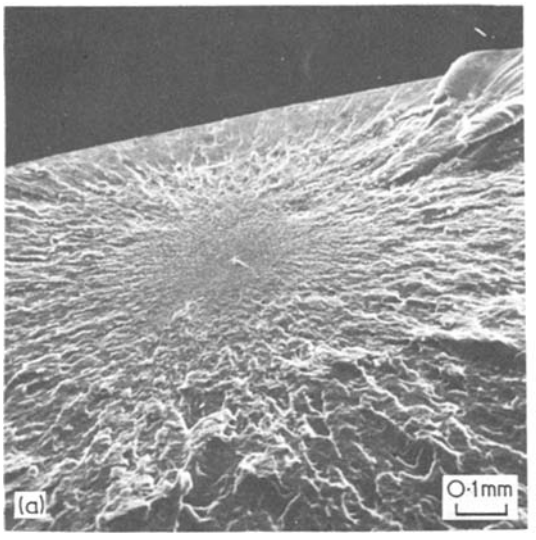

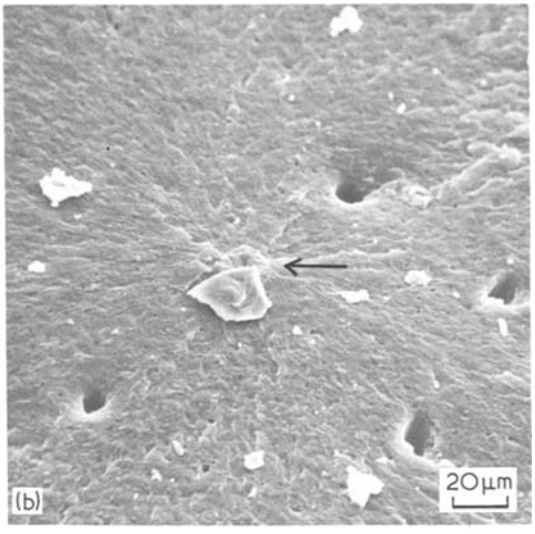

Figure 10 (a) High-temperature moulded PA.66 (b) Low V_f LCN.

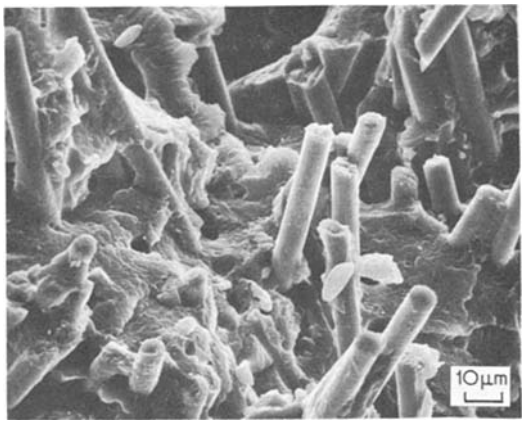

Figure 11 LCN fracture surface.

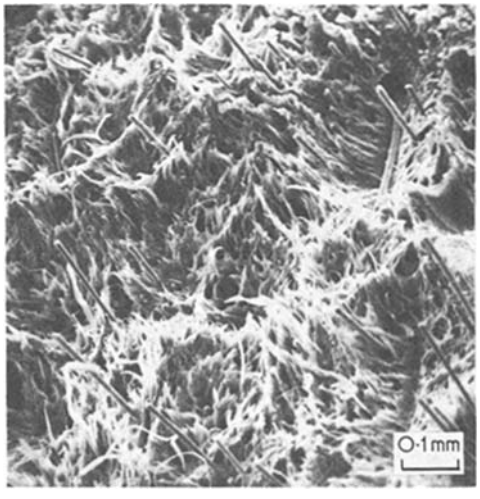

Figure 12 Ductile low V_f LCN.

Estimates of the fibre/matrix bond strength were made from measurements of fibre pull-out lengths. The maximum fibre pull-out length should be equal to the semi-critical fibre length; thus using Equation 2 the bond strength τ was evaluated, standard values for the fibre strength and radius being used. Results are summarized in Table V, together with values calculated by a method described elsewhere [1]. No variation of τ with V_f was detected and agreement between the two methods was good. Values for the carbon-filled materials were very high, substantially more than either the matrix shear yield stress (41 MN m^{-2} or its tensile yield stress (69 MN m^{-2}).

4. Discussion

4.1. Interpretation of stress/strain behaviour

The stress/strain curve shown in Fig. 1 is typical of the materials tested and shows three distinct

TABLE V Bond strengths of filled PA.66.

Material	SEM pull out length (fibre radii)	Bond strength from SEM (MN m^{-2})	Bond strength (1–4) (MN m^{-2})
Carbon fibre/ PA.66	12.5 ± 25	115 ± 25	130 ± 30
Glass fibre/ PA.66	18 ± 3	58 ± 11	65 ± 15
Commercial A190 Glass fibre/ PA.66	23 ± 4	45 ± 8	45

stages. The first stage is linear, the second parabolic and the third more complex in nature. In Stage 1 the behaviour is essentially that of a continuous fibre composite, but with fibre misalignment accounted for [7]. At very low strains, when the effects of stress build up from the fibre ends may be neglected, the stiffness, E_c, is given by a simple rule of mixtures equation which includes a fibre alignment factor C:

$$E_c = CE_fV_f + E_m(1 - V_f). \quad (1)$$

On increasing the composite strain, the shorter fibres will, at relatively low strains, cease to contribute further to the load-bearing capacity of the material [1–3]. The critical fibre length for this behaviour at a particular composite strain ϵ_c, is L_e, where

$$L_e = \frac{\sigma_f r_f}{\tau} = \frac{\epsilon_c E_f r_f}{\tau} \quad (2)$$

The stress on the composite at a strain ϵ_c may thus be given by Equation 3, where the $(1 - L_e/2\bar{L})$ term accounts for the effects of stress build-up at fibre ends [8, 9] where σ_f and σ_m are fibre and

$$\sigma_c = C\sigma_fV_f\left(1 - \frac{L_e}{2\bar{L}}\right) + \sigma_m(1 - V_f) \quad (3)$$

matrix stresses and $\bar{L}$ the mean fibre length. This is valid as long as the mean fibre length substantially exceeds L_e (as was confirmed by experiment). By assuming strain compatibility in the composite ($\epsilon_f = \epsilon_m = \epsilon_c$) and substituting for L_e from Equation 2 we arrive at the following equation for the stress/strain behaviour:

$$\sigma_c = \epsilon_c[CE_fV_f + E_m(1 - V_f)] - \epsilon_c^2\left[\frac{CE_f^2r_fV_f}{2\bar{L}\tau}\right]. \quad (4)$$

This equation predicts a parabolic behaviour, as observed experimentally in Stage 2 (Fig. 1).

By rearranging Equation 1, the orientation constant C may be calculated from the measured composite modulus and a knowledge of the fibre and matrix properties and this is shown as a function of V_f in Fig. 13. Fibre alignment apparently increases with increasing V_f, which agrees with the qualitative assessment of optical micrographs.

The Stage 2 modulus will fall with increasing strain since L_e is itself a function of strain and

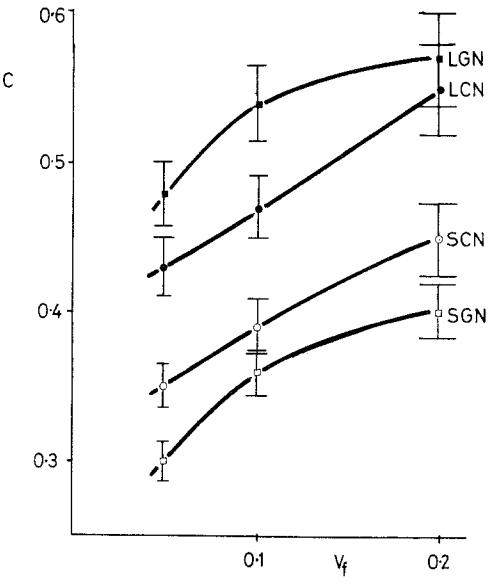

Figure 13 Variation of orientation constant C with V_f.

the term $(1 - L_e/2\bar{L})$ falls below unity. Since the transition between Stages 1 and 2 is gradual, an arbitrary change-over point has been defined when

$$\left(1 - \frac{L_e}{2\bar{L}}\right) = 0.95 \quad (5)$$

The values of strain at this transition were calculated by substituting the value of L_e from Equation 5 into Equation 2. These values are compared with the experimental values taken from the stress/strain curve (Fig. 14). Agreement is shown to be quite good for long fibres, but not so good for shorter ones. This is probably due to the poorer fibre alignment in the short fibre material and the inadequacy of a single constant C for describing large degrees of misalignment. The original assumptions imply that the transition strain is independent of C, but this is an oversimplification. The stress carried by misaligned fibres has been assumed by Cox [7] to reduce to $C\sigma_fV_f$, but to include this in the rule of mixtures equation implies that strain compatibility still exists in the composite. This has been shown by Krenchel [10] to be false, the fibre strain being reduced to $\epsilon_c \cos^2\theta$, where θ is the angle between the fibres and the loading direction.

This introduces a small error into the calculations, amounting to 3% at $\theta = 10°$ and 12% for $\theta = 20°$, thus the analysis presented would be expected to fit less well with experiment in the

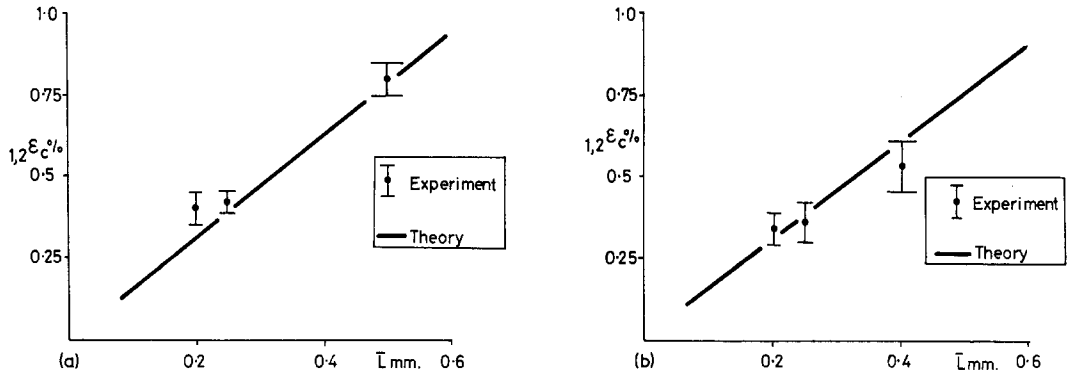

Figure 14 (a) Stage 1–2 transition strain versus mean fibre length $\bar{L}$ for glass fibre/PA.66, (b) stage 1–2 transition strain versus mean fibre length $\bar{L}$ for carbon fibre/PA.66.

less well aligned (short) fibre systems, as is indeed observed. No V_f dependence of ${}_{1,2}\epsilon_c$ is predicted, although in very low V_f systems (<0.05) the theory appears to fit less well since the matrix is less constrained by fibres and thus able to strain more overall than the average fibre strain in the test direction (i.e. the strain compatibility assumption does not hold).

The shape of the stress/strain curve is thus determined by three effects. At very low strains all the fibres are sufficiently long that the material behaves essentially as a continuous but misaligned fibre composite and Equation 1 applies. Over this range the material is virtually Hookean. Stage 2 follows from Stage 1 at a value of strain which depends on the length and degree of misorientation of the fibres, and the strength of the interface. The curve is parabolic over this region and Equation 4 applies, at least for relatively long-fibre materials where use of an average fibre length $\bar{L}$ may be justified. As the strain is increased so the shorter and more misaligned contribute less effectively to the stiffness of the composite.

Stage 3 is essentially a continuation of Stage 2 but with an additional "matrix damage" effect. The stiffness is progressively reduced by matrix cracks which form at the ends of fibres as detected by acoustic emission and optical microscopy. This process starts during the Stage 2 region and its extent is indicated qualitatively by the acoustic emission count. As the point of failure is approached this third process becomes dominant and it is this that determines the ultimate strength of the material.

4.2. Matrix cracking and ultimate failure behaviour

The onset of matrix cracking is indicated by the accoustic emission count and has been confirmed by microscopy. The most probable site for matrix crack formation is at fibre ends, which are numerous in FRTP and have been shown to substantially concentrate the stress in the adjacent matrix [11–13], producing stress magnifications of ten or even higher. The effects of these stress concentrations can be relieved only by matrix flow, fibre debonding or matrix fracture. The fibre matrix bond strengths were shown to be high in these systems and no debonding has been observed experimentally, implying that matrix yielding or cracking are the most probable mechanisms. But in all the highly filled composites brittle matrix failure has been observed and even local matrix yielding is considered unlikely. The model proposed is that as the stress is increased on the material, small cracks form at fibre ends, initially at the longest aligned fibres since these carry the highest stress, then at shorter and more misaligned fibres. Final failure will occur when catastrophic crack propagation is initiated. This might be on the formation of the first crack, or, if some cracks can be contained by stress redistribution, when a critical accumulation of cracks has developed. The observation of progressive matrix cracking suggests that the latter hypothesis is the more valid.

Consider a simple discontinuous fibre composite (Fig. 15) in which all the fibres are perfectly aligned, of equal dimensions, with $L \gg L_e$, and possess similar end geometry so that all ends

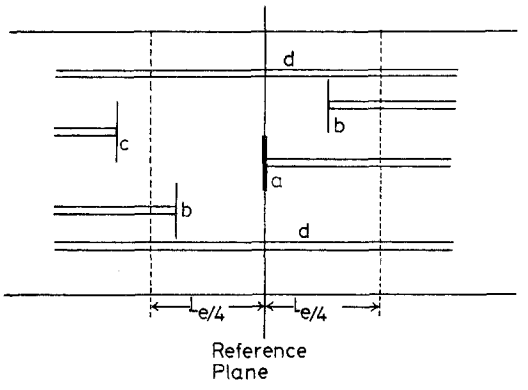

Figure 15 Failure model. (a) Fibre end on reference plane. (b) Fibre ends within $\pm L_{e/4}$ of reference plane. (c) Fibre ends outside reference zone. (d) Bridging fibres.

magnify the matrix stress to the same extent. Also assume that fibre ends are randomly dispersed throughout the composite and no interaction occurs between fibres which might raise the stress level in the matrix above that induced by a single fibre end. On loading this ideal composite, at a unique strain ϵ_i a crack will be formed at every fibre end. The initial requirement is to show that the composite is capable of surviving this sudden weakening. The stress on any plane cross-section perpendicular to the applied stress will be locally perturbed by matrix cracks, which will reduce its load bearing capacity. The nature of the perturbation is difficult to assess in an inhomogeneous system such as this, but a simple approximation can be made. In a fibre composite, fibre effects interact over a maximum distance equal to the semicritical length, but on average interactions occur over half this distance, i.e. $\pm L_e/4$. This is shown in Fig. 15 which shows fibre ends and bridging fibres across the reference zone. Fibre ends with cracks within this distance of the reference plane will be assumed to reduce its load bearing contribution by an amount equal to the crack area and if this reduced cross-section can sustain the applied load, by redistributing the load to bridging fibres the applied stress must be further increased before failure and the crack will, therefore, not lead to immediate catastrophic failure.

The number of fibre ends q_c in this volume $L_e/2$ is given by Equation 6 where Equation 2 has been used to substitute for L_e

$$q_c = \frac{V_f E_f \epsilon_c}{\pi r_f \tau L} . \tag{6}$$

A crack initiated at a fibre end propagates away from the fibre into less strained matrix, since the fibre end stress concentration decreases with increasing distance from the fibre end. At some point the crack will be halted and for the purposes of this model it is assumed that the crack will be stopped when it reaches the adjacent fibres. The maximum possible crack radius, r_s, is thus equal to the fibre surface to centre spacing and is simply related to the fibre radius and V_f. The area of a single crack, A_s, is given by Equation 7. The total crack area perturbing one plane is thus $q_c A_s$.

$$A_s = \pi \left[\left(\frac{\pi r^2}{V_f} \right) - r_f \right]^2 \tag{7}$$

In this one plane there are a certain number of continuous fibres bridging the section and still supporting load q_B, found by subtracting q_c from the total number of fibres in one cross-section. These fibres must now be capable of supporting the applied load across the weakened plane, and a new effective volume fraction, V_f^{eff},

$$V_f^{eff} = q_B \pi r_f^2 = V_f - V_f E_f \epsilon_c r_f / \tau L \tag{8}$$

can be defined (Equation 8):

$$V_m^{eff} = 1 - q_c A_s - V_f^{eff} \tag{9}$$

At the matrix cracking strain, just prior to cracking, a stress σ_{ci} is carried by the composite (Equation 10). The fracture stress of the composite depends on the strength of the most weakened section, which is

$$\sigma_{ci} = \epsilon_i E_f V_f \left[\frac{1 - E_f \epsilon_i r_f}{2L\tau} \right] + \epsilon_i E_m V_m , \tag{10}$$

determined by the bridging fibres and uncracked matrix, and is given by Equation 11. Failure occurs when the strain in the bridging fibres in the most damaged region is ϵ_{uf}, although the overall composite strain in high V_f materials may not reach this value.

$$\sigma_{uc} = \epsilon_{uf} E_f V_f^{eff} \left[1 - \frac{E_f \epsilon_{uf} r_f}{2L\tau} \right] + \epsilon_{uf} E_m V_m^{eff} \tag{11}$$

The condition for the composite to withstand matrix cracking at ϵ_i is that σ_{uc} should exceed σ_{ci}. The values of these parameters have been calculated for the materials tested, assuming

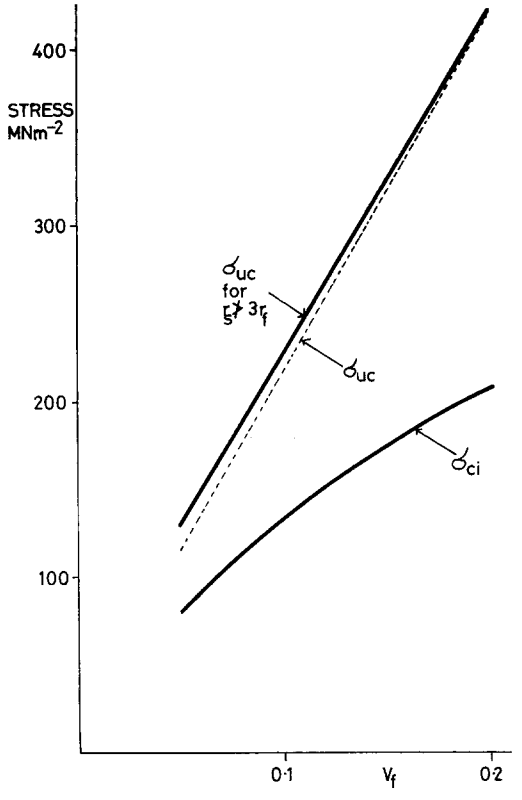

Figure 16 Comparison of calculated values of σ_{Ci} and σ_{uc} versus V_f for aligned LCN.

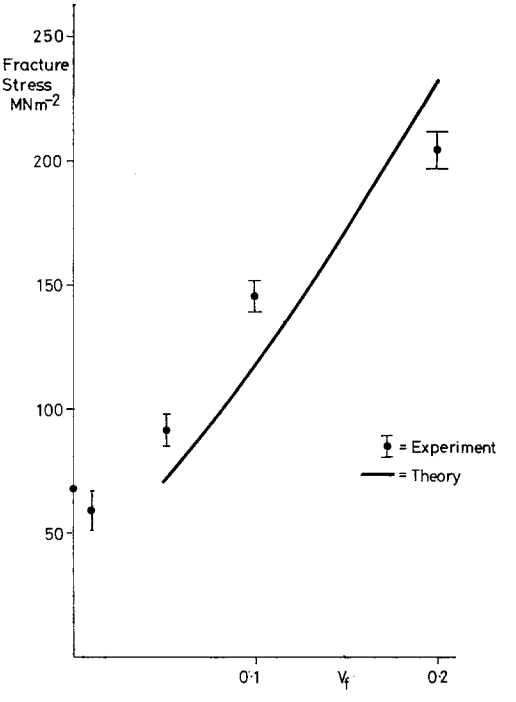

Figure 17 Comparison of experimental and theoretical values of σ_{uc} versus V_f for LCN.

fully aligned fibres ($C = 1$), taking ϵ_i to be equal to the strain for 100 counts of acoustic ouput and ϵ_c equal to the fibre failure strain. However, observations by optical microscopy showed that matrix cracks do not usually exceed more than about three fibre radii prior to fracture, and a second set of calculations used this value. A typical plot of σ_{uc} and σ_{ci} versus V_f, for LCN is shown in Fig. 16. This shows that according to the materials are capable of withstanding matrix cracking, and this agrees with experimental observation.

In real FRTP systems with misaligned fibres of a range of length, cracks form initially at long aligned fibres and then at increasing strains at more misaligned and shorter fibres, hence a unique ϵ_i would not exist. In addition, matrix cracks might not develop at all in systems containing many subcritical length fibres when this hypothesis would clearly not be applicable. It applies only to systems in which the fibre length is substantially longer than critical, such as both LCN and SCN system, but not the SGN or CGN materials.

Equation 11 may be modified to predict failure stresses in FRTP, by scaling down the fibre contribution with the orientation parameter C and use of the mean fibre length for L. The values of σ_{uc} calculated for the three appropriate systems are presented in Figs. 17 to 19 as a function of V_f, together with experimental values. Values of σ_{uc}

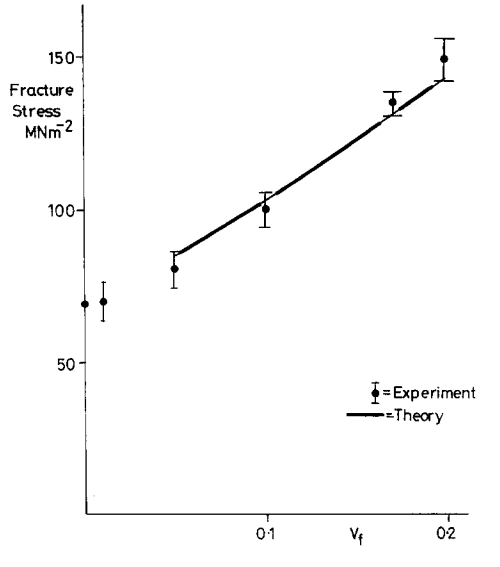

Figure 18 Comparison of experimental and theoretical values of σ_{uc} versus V_f for LGN.

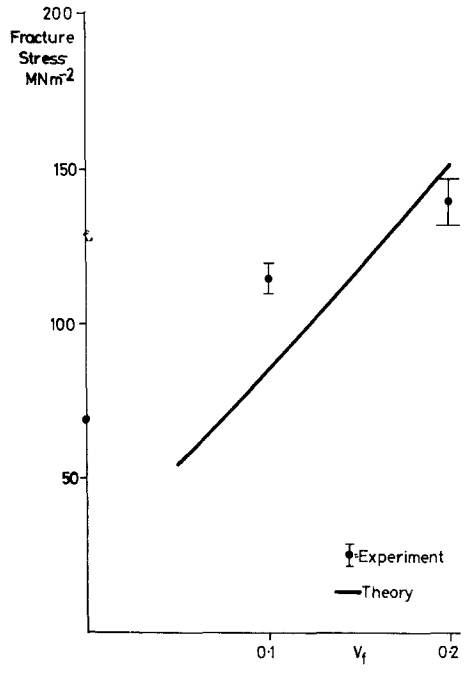

Figure 19 Comparison of experiments and theoretical values of σ_{uc} versus V_f for SCN.

were also calculated using the upper limit to r_s, resulting in a second set of predicted values. Agreement between theory and experiment is good, particularly when employing the upper limit to r_s, although in general the theory underestimates at low V_f and overestimated at high V_f. The reason for the latter may be due to neglecting fibre/fibre interactions and also local stress concentrations at the tip of matrix cracks, which might result in premature fibre failure, although this obviously depends on the ability of real fibres to debond and transfer the load over greater lengths of fibres. Deviations at low V_f are probably due to overestimation of crack area, the crack undoubtedly not propagating to adjacent fibres. At low V_f limited matrix flow may also be possible, blunting matrix cracks.

Many of the experimental observations are consistent with this matrix cracking theory. Thus failure strain falls with stiffer, longer or better aligned fibres; all these effects would lead to higher matrix stress concentration and thus formation of matrix cracks at relatively lower strains. In high V_f composites there are relatively more fibre ends and thus a larger number of matrix cracks are formed, this will also lead to failure at lower strains.

The stiffer carbon fibres lead to the formation of matrix cracks at lower strains than is the case for glass. At the other end of the scale in low V_f, short fibre materials there is the possibility of the stresses at the fibre ends being accommodated by local matrix flow to some extent so that failure strain is higher than might otherwise be predicted.

5. Conclusions

The low strain stiffness of thermoplastics may be increased by use of fibrous reinforcement. The extent of reinforcement is increased by using high V_f, longer fibres in relation to the critical length and with better fibre alignment in the test direction. These parameters also lead to higher strength but this is limited by a reduction in failure strain, which appears to follow an inverse relationship with stiffness enhancement.

The low strain behaviour of FRTP may be explained by a three-stage model. Stage 1 being a quasi-elastic regime applicable up to strains of 0.3 to 0.8% according to fibre type, length and V_f. Stage 2 is a parabolic relationship determined by the effects of the fibre ends and in Stage 3 matrix cracking further reduces the load bearing capacity of the system.

A model for the failure of these materials is proposed in which the composite is considered to be progressively weakened by cracks in the matrix at the ends of fibres. These are considered to form first (i.e. at lowest strain) at the longer more aligned fibres and to progressively spread to the shorter, less well-aligned fibres. Final failure occurs when the accumulation of cracks in a critical cross-section so weakens the material that the fibres bridging that section are unable to continue to support the load and fracture.

In the more highly reinforced materials studied the final failure strain was generally less than that of the fibres, and fibre failure was not observed other than as a consequence of the final catastrophic failure sequence.

It has been observed that the matrix in the fibre-filled material generally fails in a brittle manner although the unfilled polymer is very ductile. This is considered to be partly due to a change in morphology (probably greater crystallinity) consequent on the necessity to employ higher moulding temperatures for the filled materials, and also to the notching effect of the fibres in which considerable stress concentration

is induced in the matrix at the fibre end and matrix flow is constrained by adjacent fibres.

Acknowledgements

The work described was carried out in the Department of Metallurgy and Materials Technology at the University of Surrey and the authors would wish to acknowledge the assistance provided by the technical staff of the Department. Thanks are also due to the Fibreglass Division of Pilkington Brothers Ltd., for the supply of glass fibre and to Morganite Modmor Ltd., for the carbon fibre. One of us (P.T.C.) was supported by a Science Research council studentship.

References

1. W. H. BOWYER and M. G. BADER, *J. Mater. Sci.* 7 (1972) 1315.
2. M. G. BADER and W. H. BOWYER, *J. Phys. D.* 5 (1972) 2215.
3. W. H. BOWYER and M. G. BADER, *Faraday Spec. Disc.* 2 (1972) 165.
4. P. T. CURTIS, Ph.D Thesis, University of Surrey, (1976).
5. W. H. HAYNES and T. L. TOLBERT, *J. Composite Mater.* 3 (1969) 709.
6. M. G. BADER and P. T. CURTIS, Conference on The Mechanical Performance of Polymers, Soc. Chem. Industry, January 1977. (Proceedings to be published in the *Brit. Polymer J.).*
7. H. L. COX, *Brit. J. Appl. Phys.* 3 (1952) 72.
8. A. KELLY, "Strong Solids", (Clarendon, Oxford, 1973).
9. A. KELLY and W. R. TYSON, *J. Mech. Phys. Sol.* 13 (1965) 329.
10. H. KRENCHEL, "Fibre Reinforcement" (Akademisk Forlag, Copenhagen, 1964) p.11.
11. G. A. COOPER, "Micromechanics Aspects of Fracture and Toughness", from "Composites" Vol. 5, edited by L. J. Broutman and R. H. Krock Academic Press, New York and London, (1974) p. 415.
12. R. M. BARKER and T. F. MACLAUGHTON *J. Composite Mater.* 5 (1971) 492.
13. M. G. BADER, P. T. CURTIS and R. S. CHHATWAL, AIME International Conference on Composite Materials, Geneva (1975).

Received 27 April and accepted 8 June 1977.